crucial for the success of the electron capture mode. Investigation of other classes of complexes that exhibit a stable lower oxidation state will be necessary, however, before the generality of this observation can be established.

Acknowledgment. We thank the CNRS (Unité Associée No. 1194: Laboratoire de Chimie de Coordination) for partial support of this research and Dr. Jean-Marc Latour for several interesting discussions.

Registry No. $TiF_2(tpp)$, 66350-84-3; $TiCl_2(tpp)$, 66350-83-2; $TiBr_2(tpp)$, 66350-82-1; TiO(tpp), 58384-89-7.

Contribution from the Departments of Chemistry, University of Notre Dame, Notre Dame, Indiana 46556, and The Ohio State University, Columbus, Ohio 43210

Substituent Effects in Clusters. 5. UV-Photoelectron Spectroscopic and Quantum-Chemical Analyses of $H_3Os_3(CO)_9BCO$, $H_2Os_3(CO)_9CCO$, and Related Clusters

R. D. Barreto,[†] T. P. Fehlner,*[†] L.-Y. Hsu,[‡] D.-Y. Jan,[‡] and S. G. Shore*[‡]

Received January 14, 1986

The gas-phase UV-photoelectron spectra of $(\mu\text{-}H)_3Os_3(CO)_9BL$ (L = CO, $P(CH_3)_3$) (IIIa,b), $(\mu\text{-}H)_2Os_3(CO)_9CCO$ (IV), and $(\mu\text{-}H)_3Os_3(CO)_9CX$ (X = C_6H_5, Cl, Br) (Ic–e) were measured by using He I radiation with the spectra of Ic and IIIa also being measured with Ne radiation. The observed bands were assigned by comparison to model compounds, intensity changes with photon energy, and exo-cluster substituent effects. The empirical results on IIIa,b and IV are intercompared in order to probe the bonding of the main-group atom to the Os_3 triangle and the interaction of CO and $P(CH_3)_3$ with a capping boron atom. Molecular orbital calculations of the Fenske–Hall type were carried out for the same molecules. The information gained is consistent with that derived from the spectroscopic work and gives further informative details of the electronic structure. Both the PES results and the MO calculations suggest that boron is acting as a pseudo metal cluster atom relative to the metal centers as well as to attached ligands.

The comparison of spectroscopic properties of isoelectronic molecules is a classical method for obtaining information on the corresponding electronic structures. Indeed such comparisons also constitute a body of data of significant pedagogical value. Although nowadays small molecule problems are effectively treated with modern quantum-chemical techniques, large systems, e.g., transition-metal clusters, are not easily dealt with. In a continuing effort we have pointed out the usefulness of comparing isoelectronic molecules that differ only in the spatial location of a proton.[1] The differences in spectroscopic properties can be related straightforwardly to the perturbation of the electronic structure caused by the proton. For example, the comparison of $H_3Fe_3(CO)_9CCH_3$ (Ia) with $Co_3(CO)_9CCH_3$ (II) (Chart I) provided a means for probing the metal–metal interactions in the capped trinuclear metal cluster system.[1b,c]

The recent preparation of the first borylidyne transition-metal cluster compound, $H_3Os_3(CO)_9BCO$[2] (IIIa), along with the existing isoelectronic counterpart, $H_2Os_3(CO)_9CCO$[3] (IV), allows the capped trinuclear metal cluster system to be further investigated. In going from IIIa to IV, a proton is formally moved from a M–M edge to the nucleus of the capping atom. With the understanding gained already from Ia and II, the comparison of IIIa and IV provides a source of information on the capping-atom–metal-triangle interaction. Further, as the CO ligand on the capping boron of IIIa has been replaced by a phosphine,[2] an opportunity is presented for exploring to what extent boron behaves as a pseudometallic cage atom. That is, are the interactions of L with the boron of IIIa,b essentially similar to or different from those of L with an osmium atom?

To explore the electronic structures of IIIa and IV, two techniques are utilized. First, UV-photoelectron (PE) spectroscopy provides an exact, but not detailed, look at some properties of the lowest lying radical-cation states of the molecule. By the use of the spectra of model compounds, spectra at two different photon energies, and exo-cluster substituent effects, the pertinent bands in the spectra are assigned.[4] The results are presented in the language of the LCAO MO model by using Koopmans' theorem[5] but in no way depend on the validity of the model or the theorem.

Chart I

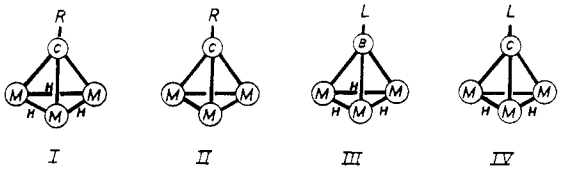

a, M = Fe, R = CH_3
b, M = Ru, R = H
c, M = Os, R = C_6H_5
d, " , R = Cl
e, " , R = Br

M = Co, R = CH_3

a, M = Os, L = CO
b, " , L = $P(CH_3)_3$

M = Os, L = CO

Second, IIIa and IV are also examined by using the Fenske–Hall technique, a nonparametrized, self-consistent-field MO method.[6] This allows a more detailed, but approximate, examination of these molecules. For both approaches the emphasis is on relative comparisons, viz. IIIa and IV, and thus the problems associated with absolute measurements or calculations are largely avoided.

Photoelectron Spectroscopic Results

General Band Assignment of IIIa. The PE spectrum of IIIa is shown in Figure 1A, and the numerical data are summarized

[†] University of Notre Dame.
[‡] The Ohio State University.

(1) (a) Wong, K. S.; Dutta, T. K.; Fehlner, T. P. *J. Organomet. Chem.* **1981**, *215*, C48. (b) DeKock, R. L.; Wong, K. S.; Fehlner, T. P. *Inorg. Chem.* **1982**, *21*, 3203. (c) DeKock, R. L.; Deshmukh, P.; Fehlner, T. P.; Housecroft, C. E.; Plotkin, J. S.; Shore, S. G. *J. Am. Chem. Soc.* **1983**, *105*, 815. (d) Vites, J. C.; Housecroft, C. E.; Jacobsen, G. B.; Fehlner, T. P. *Organometallics* **1984**, *3*, 1591.
(2) Shore, S. G.; Jan, D.-Y.; Hsu, L.-Y.; Hsu, W.-L. *J. Am. Chem. Soc.* **1983**, *105*, 5923.
(3) Shapley, J. R.; Strickland, D. S.; St. George, G. M.; Churchill, M. R.; Bueno, C. *Organometallics* **1983**, *2*, 185.
(4) (a) Turner, D. W.; Baker, C.; Baker, A. D.; Brundle, C. R. *Molecular Photoelectron Spectroscopy*; Wiley: New York, 1970. (b) Rabalais, J. W. *Principles of Ultraviolet Photoelectron Spectroscopy*; Wiley-Interscience: New York, 1977.
(5) Koopman, T. *Physica (Amsterdam)* **1934**, *1*, 104.
(6) (a) Hall, M. B.; Fenske, R. F. *Inorg. Chem.* **1972**, *11*, 768. (b) Hall, M. B. Ph.D. Thesis, University of Wisconsin, Madison, WI, 1971. (c) Fenske, R. F. *Pure Appl. Chem.* **1971**, *27*, 61.

0020-1669/86/1325-3572$01.50/0

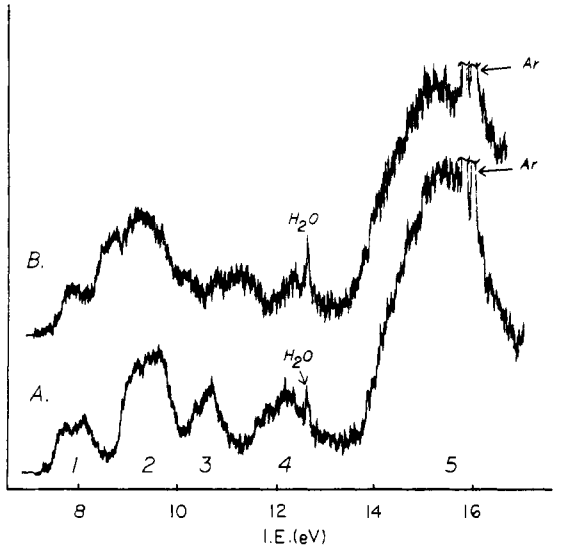

Figure 1. He I PE spectra of (A) $H_3Os_3(CO)_9BCO$ and (B) $H_2Os_3(CO)_9CCO$.

in Table I. A general assignment of the bands proceeds in the same manner as previously seen for Ia.[1] The published spectrum of $Os_3(CO)_{12}$[7] demonstrates that bands 1 and 2 arise from MO's of high metal d character and band 5 arises from MO's of high CO ligand character. Likewise, the published spectra of $H_3Re_3(CO)_{12}$ and $H_2Os_3(CO)_{10}$[7,8] suggest that band 4 is due to ionization potentials (ip's) having high M–H–M character, an observation that is confirmed by the variation in the intensity of band 4 relative to band 2 in going from He I to Ne I radiation. By difference, band 3 is assigned to ip's associated with the capping atom. The shoulder that is present on the low-energy side of this band is assigned to a d-band ionization. Bands of this character have been seen at this energy in $Os_3(CO)_{12}$, $H_2Os_3(CO)_{10}$, and $H_4Os_4(CO)_{12}$.[7b]

A good estimate of the number of ip's expected in the energy range of Figure 1 can be obtained by simply summing the populations of the constituent atoms contained in atomic orbitals with energies less than 16 eV, i.e. the 6s and 5d of Os, the 2p of all the main-group atoms, and the 2s of boron.[9] This yields 45 pairs and suggests an equivalent number of ip's are represented by the spectrum of IIIa in Figure 1. Of these 30 are to be associated with the CO ligands (band 5). Of the remaining 15, simple orbital analyses of the $Os(CO)_3$ fragment would suggest nine ip's associated with the metal "t_{2g}" levels (bands 1, 2, and part of 3) leaving six ip's for the cluster bonding (part of band 3 and band 4). The latter are associated with the three OsHOs and three OsB interactions. This crude assignment is supported by the relative band areas (Table I). These areas also suggest that band 1 contains three ip's. Further, the shape of band 1 suggests two ionization events of relative intensity of 1:2, i.e., ip's corresponding to an a and e symmetry MO set. However, the Ne I data suggest in addition that band 1 as well as bands 3 and 4 contains significant main-group character. Hence this overall assignment needs refinement if the metal–boron interaction is to be revealed.

Substituent Perturbations. In C_{3v} symmetry the six cluster ip's referred to above will result from ionization of sets of MO's having e and a symmetry. The OsHOs interactions are expected in a single e + a set whereas the OsB interactions may well be found in more than one e + a set.[7] Indeed a study of Ib suggests as much.[10] Identification of the e manifold (odd functions with respect to the two mutually perpendicular planes containing the

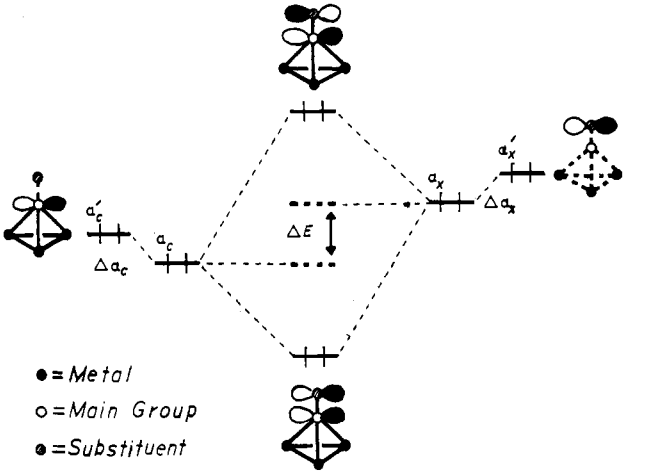

Figure 2. General interaction diagram for a substituent molecular orbital with one e symmetry cluster orbital.

Chart II

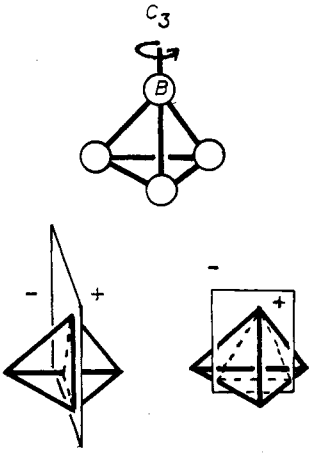

C_3 axis—see Chart II) associated with boron is particularly important for the investigation of the nature of the boron–ligand interaction. If boron mimics a metal there should be significant back-donation from the Os_3B cluster into the π orbital of the CO ligand attached to boron in IIIa. This type of interaction would take place via the e manifold associated with boron and provides the impetus for experimentally locating these ip's.

We have demonstrated several times previously that exo-cluster substituent effects can be used to unambiguously identify ip's arising from MO's of e symmetry.[11] Briefly, attachment of a substituent containing filled MO's of π symmetry with respect to the bond axis of attachment results in a 2-fold perturbation of the cluster MO's.[12] As illustrated schematically in Figure 2 for single cluster and substituent MO's having energies $-\alpha'_c$ and $-\alpha'_x$, the first perturbation corresponds to an inductive effect causing shifts in the MO energies of $\Delta\alpha_c$ and $\Delta\alpha_x$. As this inductive effect is relatively small and affects all the MO's it is not useful for distinguishing MO's of different character. The second perturbation is a conjugative effect that results from the direct interaction of symmetry-compatible orbitals on the cluster and substituent. This effect can be large and selective. As illustrated schematically for a capped, C_{3v} symmetry, trinuclear metal cluster, this conjugative interaction will be significant for substituents on the main-group capping atom. The observed splitting will depend inversely on ΔE and can be parametrized with α_c, α_x, and β. Substituents can be chosen such that ΔE is varied; thus, one or both components of an e set can be subjected to a conjugative substituent shift.

(7) (a) Green, J. C.; Mingos, D. M. P.; Seddon, E. A. *J. Organomet. Chem.* **1980**, *185*, C20. (b) Green, J. C.; Mingos, D. M. P.; Seddon, E. A. *Inorg. Chem.* **1981**, *20*, 2595.
(8) Sherwood, D. E.; Hall, M. B. *Inorg. Chem.* **1982**, *21*, 3458.
(9) Carlson, T. A.; Nu, C. C.; Tucker, T. C.; Nestor, C. W., Jr.; Malik, F. B. Report ORNL-4614; Oak Ridge National Laboratory: Oak Ridge, TN, Dec 1970.
(10) Sherwood, D. E.; Hall, M. B. *Organometallics* **1982**, *1*, 1519.
(11) (a) Ulman, J. A.; Fehlner, T. P. *J. Am. Chem. Soc.* **1976**, *98*, 1119. (b) Beltram, G. A.; Fehlner, T. P. *J. Am. Chem. Soc.* **1979**, *101*, 6237.
(12) Bock, H.; Ramsey, B. G. *Angew. Chem., Int. Ed. Engl.* **1973**, *12*, 734.

Table I. He I Photoelectron Spectroscopic Data[a]

band	IIIa ip,[b] eV	IIIa no. of ip's	IIIa area[c,d] He	IIIa area[c,d] Ne	IIIb ip,[b] eV	IIIb no. of ip's	IIIb area[c]	IV ip,[b] eV	IV no. of ip's	IV area[c]	Ic ip,[b] eV	Ic no. of ip's	Ic area[c,d] He	Ic area[c,d] Ne	Id ip,[b] eV	Id no. of ip's	Id area[c]	Ie ip,[b] eV	Ie no. of ip's	Ie area[c]
1	(7.34)		3	4	(6.76)		2	(7.61)			(7.03)				(7.50)		3	(7.63)		3
	7.86 sh	1			7.09 sh	1		8.00	1	1	7.35	2	3	3	7.87 sh	1		7.87 sh	1	
	8.22	2			7.54	2		8.88	3	3	8.08	1			8.28	2		8.32	2	
2	9.69	5	8	8	8.70	5	8	9.80	5	8	9.32	7	12	14	9.50	5	8	9.43	5	8
3	10.75	2	4	5	10.13	6	6	10.83	1	4	10.64	3	4	8	10.67	2	5	10.34	2	5
	10.34 sh	1						11.37	2						10.86 sh	1		10.70 sh	1	
4	11.86 sh	4	6	9	11.3	4	6	12.36	2	3	11.99	6	13	21	12.29	5	9	11.51	5	9
	12.20				11.7													12.09		
5	15.22	≥28	37	*e*	14.98	≥28	37	15.22	≥28	*e*	14.97	≥28	*e*	*e*	15.57	≥28	*e*	15.58	≥28	*e*

[a] See figures. [b] Vertical ip's. Adiabatic ip's are in parentheses; sh ≡ shoulder. [c] Uncorrected for instrument function. [d] Underlined areas were set equal. [e] Not measured.

Table II. Parameters (eV) Used To Fit the Spectra of Ic–e

	$-\alpha_{1cage}$	$-\alpha_{2cage}$	$-\alpha_x$	$-\beta_1$	$-\beta_2$
C_6H_5	8.0	10.5	8.8	0.8	0.6
Cl	8.5	11.0	11.6	0.8	0.6
Br	8.5	11.0	10.8	0.8	0.6

Table III. Fit of Ionization Potentials (eV)

Ic obsd	Ic calcd	Id obsd	Id calcd	Ie obsd	Ie calcd
7.35	7.5	8.28	8.3	8.3	8.2
8.08	8.0	10.67	10.7	10.3	10.5
9.0	8.8, 9.1	12.29	12.1	11.5	11.6
10.64	10.5, 10.7				

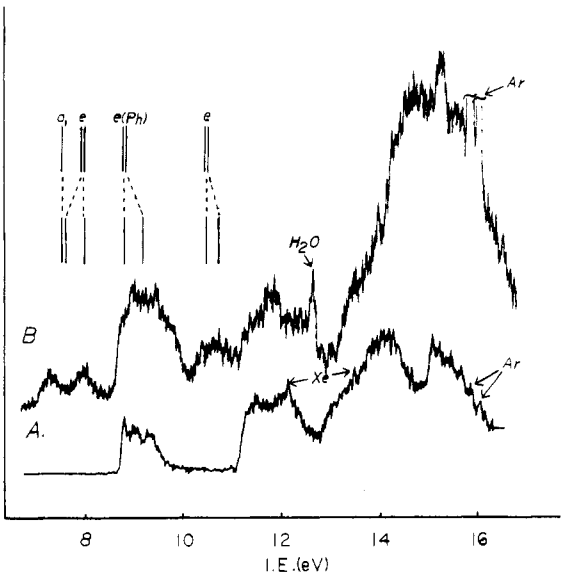

Figure 3. He I PE spectra of (A) toluene and (B) $H_3Os_3(CO)_9CC_6H_5$ with predicted band positions and splitting for part B.

This approach is applied to Ic–e. As the general assignments of the spectra of I and III are essentially the same, the resulting assignment will be valid for both. We begin with Ic, which contains a phenyl substituent. The substituent orbital of interest is the ring π set with an ip of 9.2 eV in benzene. As one of these MO's has a node at the position of substitution, only one can interact in a conjugative manner with the cluster orbitals. As a result, orbitals of e symmetry will be split. A more complete description of phenyl substituent effects on metal cluster systems will be found elsewhere.[13]

The spectra of Ic are shown in Figure 3 and the numerical data are given in Table I. A spectrum of $C_6H_5CH_3$ shown at the bottom of Figure 3 demonstrates the approximate location of the substituent π ip's (9 eV) as well as the fact that the other substituent ip's restrict our analysis to bands 1–3 of I. The Ne I spectrum of Ic suggests the presence of the π ip's on the low-ip side of band 2. Band 1 of Ic appears as two well-split components of approximately equal area, and band 3 is broad. Both observations suggest conjugative substituent–cluster interactions. The energies of the three bands (band 1, the substituent component of band 2 and band 3) can be parametrized by using the model described above. The parameters chosen are given in Table II, and the fit is shown in Figure 3. The values of the parameters are all reasonable but, obviously, do not constitute a unique set. The qualitative conclusion is that bands 1 and 3 of I (and III) contain (in C_{3v} symmetry) e sets with significant capping atom character. In addition, band 1 also contains another ip, most likely resulting from an a_1 MO.

Confirmation of this assignment as well as the parametrization results from an examination of the spectra of the halogenated derivatives, Id,e. In these cases the halogen lone pairs constitute a set of filled orbitals that interact identically with both components of the e sets of the cluster. The spectra of Id,e are shown in Figure 4, and the data are contained in Table I. In both cases the halogen substituent results in additional band intensity in bands 3 and 4. Numerous studies of halogenated compounds demonstrate that this added intensity is due to the halogen "lone pairs" and that no other ip's from the substituent are expected in the region covered by bands 1–4.[10,11,14] From past work we know the difference between α_{Cl} and α_{Br} is 0.8–0.9 eV, α_{Cl} lies between −11.5 and −12.2 eV, and β ranges from −0.5 to −1.0.[11] The a_1 ip in band 1 of Ic–e can be used to estimate the difference in

(13) DeKock, R. L.; Deshmukh, P.; Dutta, T. L.; Fehlner, T. P.; Housecroft, C. E.; Hwang, J. L.-S. *Organometallics* **1983**, *2*, 1108.
(14) (a) Granozzi, G.; Tondello, E.; Ajo, D.; Casarin, M.; Aime, S.; Osella, D. *Inorg. Chem.* **1982**, *21*, 1081. (b) Chesky, P. T.; Hall, M. B. *Inorg. Chem.* **1981**, *20*, 4419.

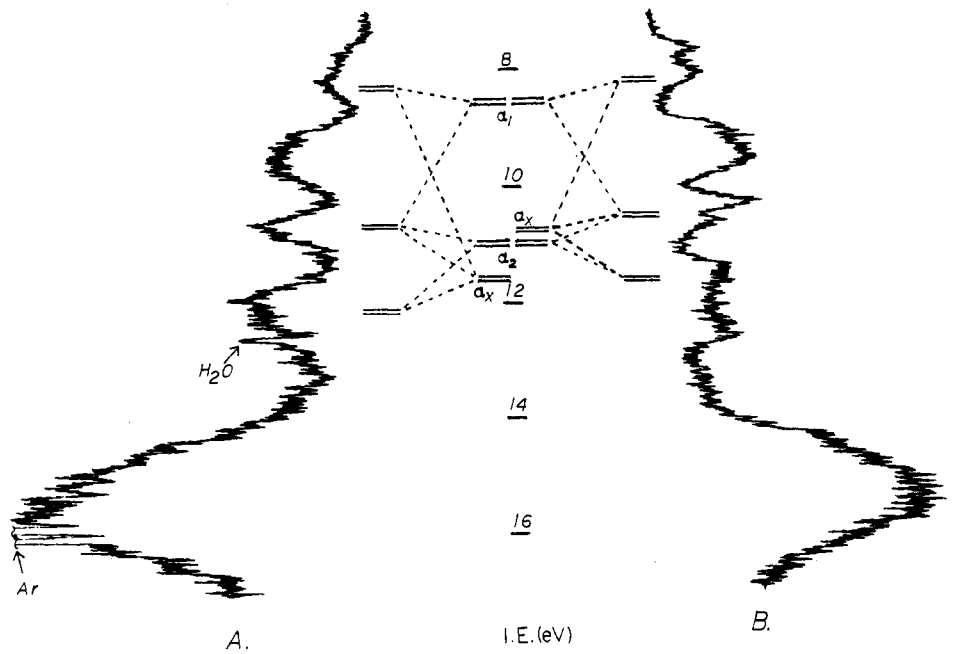

Figure 4. He I PE spectra of (A) $H_3Os_3(CO)_9CCl$ and (B) $H_3Os_3(CO)_9CBr$ with the predicted band positions for each compound.

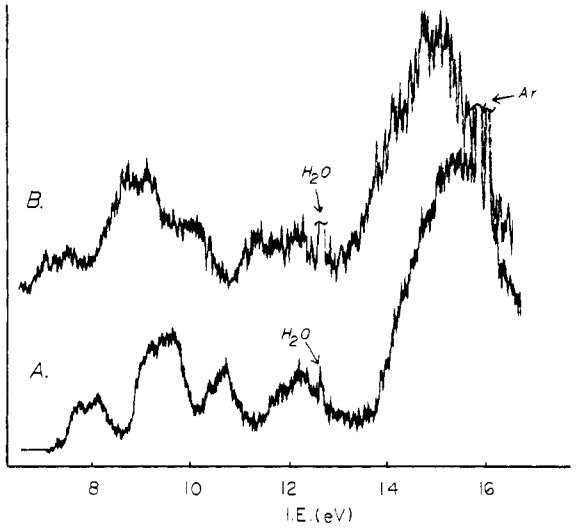

Figure 5. He I PE spectra of (A) $H_3Os_3(CO)_9BCO$ and (B) $H_3Os_3(CO)_9BP(CH_3)_3$.

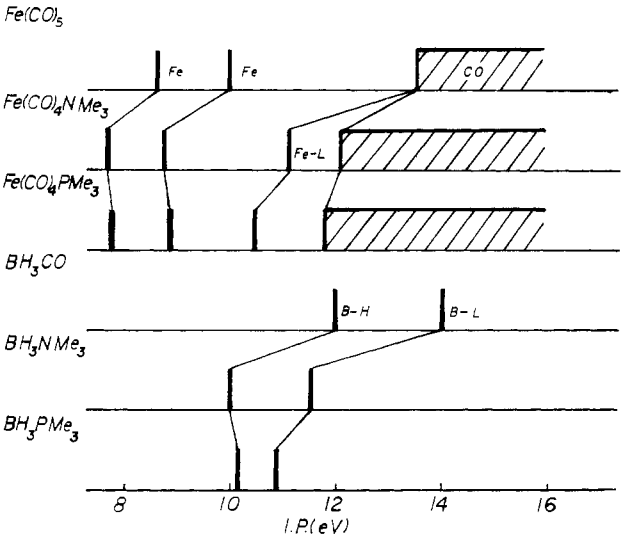

Figure 6. Schematic representation of the PE spectra of the indicated compounds demonstrating the inductive effect of various ligands in BH_3–L and $Fe(CO)_4$–L systems.

inductive effect between phenyl and the halogens. For a cluster inductive shift of 0.5 eV, the same β values as used for Ic, α_{Cl} of −11.6 eV, and $\alpha_{Cl} - \alpha_{Br} = 0.8$ eV, the band positions are fit as shown in Figure 4. A summary of the parameters used is given in Table II and a numerical comparison of the calculated and measured band positions is given in Table III. The fact that a satisfactory fit is obtained with an internally consistent set of parameters confirms that both bands 1 and 3 of I (and III) contain ip's resulting from e symmetry MO's containing significant capping atom character. The β parameters used would suggest that the interaction between α_x and α_{1cage} is greater than that between α_x and α_{2cage}.

Nature of the Boron–Ligand Interaction. Having located those ip's that contain high boron character and that will be most sensitive to ligand π-type back-bonding interactions, we can now investigate the boron–ligand interaction by comparing the spectra of IIIa,b, i.e. replacing CO, a poor σ donor and a good π acceptor, with $P(CH_3)_3$, a better σ donor and a poorer π acceptor. The two spectra are compared in Figure 5, and the data for IIIb are given in Table I. The spectrum of IIIb is similar to that of IIIa except for additional band intensity lying between bands 2 and 3. By reference to model compounds, e.g. $BH_3P(CH_3)_3$, these additional ip's are attributed to the two P–C and one B–P ip's expected. With this exception, the spectra are virtually superimposable if IIIa is shifted 0.6 eV to lower ip. That is, there is no differential stabilization/destabilization of the bands derived from the e manifold.

The interpretation of these observations is made by reference to spectra of model systems. Consider first the series BH_3L, with L = CO, $P(CH_3)_3$, and $N(CH_3)_3$ (Figure 6).[15] As one goes from poor (L = CO) to better σ donors, the band corresponding to ionization of the e(BH) MO's decreases 1.85 (P donor) and 2.0 eV (N donor). In this system the BH_3 fragment has no means of offloading the charge from the base; hence, these ip changes are a measure of the substituent effect expected on the boron-centered orbitals in the absence of any mechanism for charge redistribution. This is corroborated by the trend in a_1(B–L) ip − L(lone pair) ip, which decreases in the series $N(CH_3)_3$, $P(CH_3)_3$, CO (3.06, 2.28, 0.14 eV).

The ligand σ and π effects on the PE spectrum of a transition-metal compound can be established in a similar fashion.

(15) (a) Lloyd, D. R.; Lynaugh, N. *J. Chem. Soc., Faraday Trans. 2* **1972**, *68*, 947. (b) Cowley, A. H.; Kemp, R. A.; Lattman, M.; McKee, M. L. *Inorg. Chem.* **1982**, *21*, 85.

Chart III

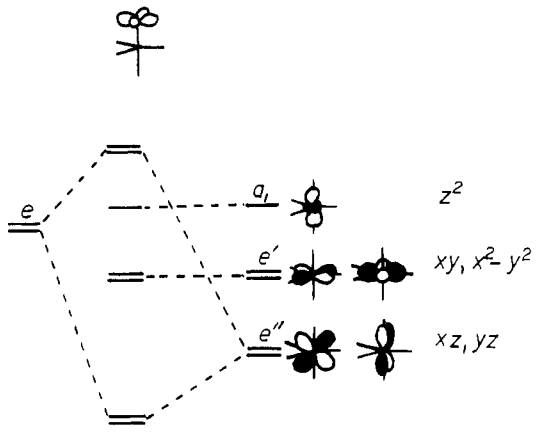

Consider the series $(CO)_4FeL$ with L in an axial position and with L = CO, $P(CH_3)_3$, and $N(CH_3)_3$. Note that $Fe(CO)_4$ is isolobal with BH_3[16] and that the PE spectra of all these compounds are known.[17] The pertinent data are schematically shown in Figure 6. To make our point the electronic structure of $Fe(CO)_5$ must be briefly reviewed. Hoffmann has presented a simplified analysis of a ML_5 system, and, for a d^8 metal with D_{3h} symmetry of the ligands: the highest occupied MO is doubly degenerate and of e′ symmetry while the next most stable MO is of e″ symmetry. (See Chart III.)[18] That these occupied MO's correspond to the first two bands in the PE spectrum of $Fe(CO)_5$ has been elegantly demonstrated by Lichtenberger by an empirical analysis of the band fine structure.[19] Note that π effects with an axial ligand are expected to affect the e″ levels more strongly than the e′ levels whereas charge effects (σ donation) should affect both about the same extent. Thus, the splitting between the e′ and e″ bands is a measure of the relative π-acceptor properties of the ligand while the relative ip of the e′ band is a measure of the σ-donor ability. As shown in Figure 6, the greatest e′–e″ splitting is observed for L = CO and the least for L = $N(CH_3)_3$ with that for L = $P(CH_3)_3$ being in between these values but not very different from that for the amine. This is in accord with the accepted back-bonding abilities of the three bases but, more importantly for our purposes, gives a measure of the magnitude of relative band shift expected in going from a good π acceptor to a poor σ acceptor, i.e. 0.2 eV. Likewise the lower ip's of the e′ ionizations for L = $N(CH_3)_3$ and $P(CH_3)_3$ reflects the greater charge buildup on the metal center due to greater net ligand to metal charge transfer. The values are again in accord with accepted ideas of the π-donor abilities of these ligands. The net decrease in the e′ ip in going from CO to $P(CH_3)_3$, 0.8 eV, is a measure of the shift expected in going from a poor σ donor to a good σ donor. Finally note that ip's of the Fe–L ionizations relative to the lone-pair ip's of the free bases exhibit the same trend observed for the isolobal BH_3L derivatives discussed initially.

Returning to the comparison of IIIa and IIIb, we are now in a position to interpret the band shifts observed. The general shift of all similar bands to lower ip in going from L = CO to $P(CH_3)_3$ is a reflection of the greater net electronic charge deposited on the cluster by the phosphine relative to CO. The fact that the shift is less than that in the mononuclear metal example and 3 times less than in the case of the borane suggests that this charge is spread out over the cluster. The fact that there is no *measurable* differential shift between the e ip's of IIIa,b suggests that the net π back-bonding is either less than that in the model mononuclear system or is spread out over more orbitals. Note, however, that this negative observation cannot be taken as evidence of the absence of a significant π-back-bonding interaction between boron and CO in IIIa. The calculations, discussed below, provide more definitive information on the boron–ligand interaction.

Nature of the Boron–Cluster Interaction. In a formal sense, going from IIIa to $H_2Os_3(CO)_9CCO$ (IV), a proton is transferred from a metal–metal edge to the main-group capping-atom nucleus. Those orbitals with large amplitudes at the metal edge losing the proton or with large boron character are expected to be significantly perturbed.

The spectra of IIIa and IV are compared in Figure 1, and the data are given in Table I. Besides a general broadening of the spectrum of IV with respect to IIIa attributed to the lower symmetry of the former, the major changes are (a) a merging of part of band 1 with 2 and an increase in band intensity, (b) a shift of band 3 to higher ip, and (c) a loss in intensity from band 4. In accord with our previous analysis of Ia and II,[16] the loss in intensity from band 4 coupled with the gain in intensity in band 1 results from the loss of a M–H–M ip and the gain of a MM ip. The 3.5-eV destabilization involved is similar to that observed in model systems, e.g. CS vs. HBS.[20] However, this shift does not account for all the intensity lost in band 4, as the areas in Table I indicate. The remaining intensity, the result of the Os_3B ionization, is shifted into band 5 and now appears as a shoulder on the low-energy side of the band. This stabilization is due to the increase in the effective nuclear charge of the capping group on going from B to C. Since this ionization has large 2s character, it undergoes a large stabilization of 1.5–2.0 eV (in going from atomic boron to atomic carbon, the first ionization undergoes a 3 eV stabilization). The approximately 0.7-eV stabilization of a component of band 1 and band 3 is also due to the increased effective nuclear charge of the capping atom (in going from B to C). The shift is smaller as the proton is now buried in a nucleus with its effect being shielded by the other electrons. The shift of bands 1 and 3 is further evidence that they contain significant capping-atom character. A more detailed view of the boron–cluster interaction results from the calculations discussed below.

Quantum-Chemical Calculations

Calculations of the Fenske–Hall type have proven to be a useful technique for the study of the electronic structure within transition-metal clusters.[6] One helpful approach using this technique is to partition a cluster molecule into fragments in order to analyze their binding modes. After SCF convergance in the atomic basis, the results can then be "transformed" into the basis set of the fragment molecular orbitals, in effect bringing the fragments together to observe how they interact. In this way, the bonding differences in isostructural and/or isoelectronic clusters can be investigated in terms of the qualitative changes that take place on going from one system to another. This technique has been employed to investigate the bonding in Ic–e, IIIa,b, and IV. Fragment analysis was performed in terms of $(\mu\text{-H})_3Os_3(CO)_9^+/BCO^-$ and $(\mu\text{-H})_2Os_3(CO)_9/CCO$ for IIIa and IV in order to compare the bonding of a metal fragment with a boron and carbon moiety. Fragment analyses of IIIa,b were also performed for $(\mu\text{-H})_3Os_3(CO)_9B/CO$ and $(\mu\text{-H})_3Os_3(CO)_9B/PMe_3$ to compare bonding to apical CO and PMe_3 ligands in boron-capped clusters.

A. $(\mu\text{-H})_3(CO)_9Os_3^+$ Compared to $(\mu\text{-H})_2(CO)_9Os_3$. Molecular orbital calculations were carried out on the isoelectronic fragments $(\mu\text{-H})_3(CO)_9Os_3^+$ (III′) and $(\mu\text{-H})_2(CO)_9Os_3$ (IV′). The energy level diagrams for III′ and IV′, assuming idealized geometries of C_{3v} and C_s, respectively, are given in Figure 7. These fragments have 58 occupied MO's considering only the valence electrons. The first 45 low-lying MO's are predominantly associated with the CO ligands. The nine orbitals 49–57 of III′ and the nine orbitals of IV′, 48–56, are associated with the 5d band, classified t_{2g}. Orbitals 46–48 of III′ and orbitals 46–47 of IV′ bind the

(16) (a) Wade, K. *Adv. Inorg. Chem. Radiochem.* **1976**, *18*, 1. (b) Mingos, D. M. P. *J. Chem. Soc., Dalton Trans.* **1974**, 133.
(17) (a) Boxhoorn, G.; Cerfontain, M. B.; Stufkens, D. J.; Oskam, A. *J. Chem. Soc., Dalton Trans.* **1980**, 1336. (b) Flamini, A.; Semprini, E.; Stefani, F.; Cardaci, G.; Bellachioma, G.; Andreocci, M. *J. Chem. Soc., Dalton Trans.* **1978**, 695.
(18) Rossi, A. R.; Hoffmann, R. *Inorg. Chem.* **1975**, *14*, 365.
(19) Hubbard, J. L.; Lichtenberger, D. L. *J. Chem. Phys.* **1981**, *75*(6), 2560.
(20) (a) Fehlner, T. P.; Turner, D. W. *J. Am. Chem. Soc.* **1973**, *95*, 7175. (b) Kroto, H. W.; Suffolk, R. J.; Westwood, N. P. C. *Chem. Phys. Lett.* **1973**, *22*, 495.

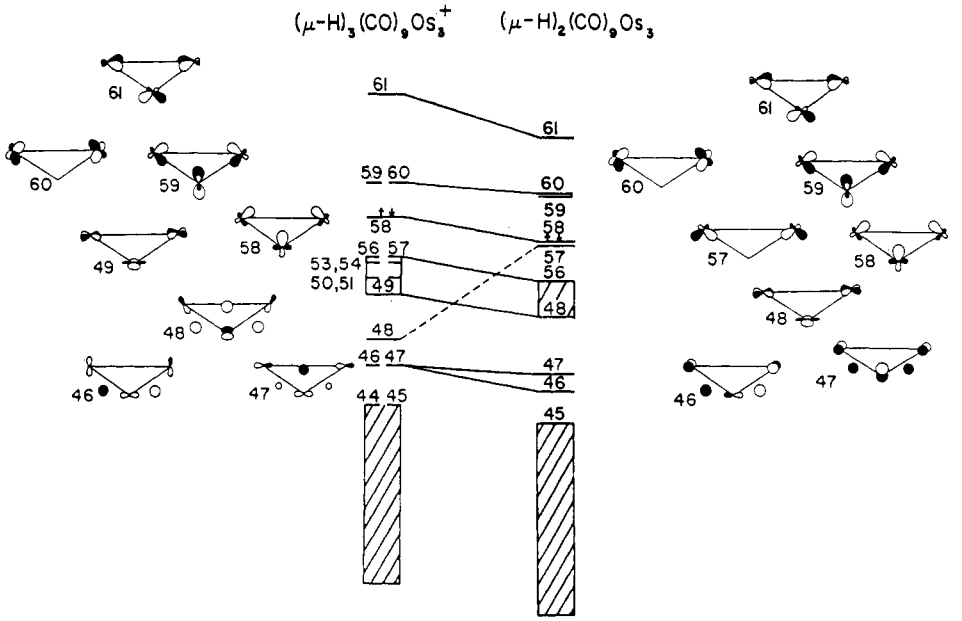

Figure 7. Schematic representation of the important orbitals of III′ and IV′ idealizing the symmetry as C_{3v} and C_s, respectively. The orbital energy changes on going from left to right are also illustrated.

Table IV. Frontier MO's of $(\mu\text{-H})_3(CO)_9Os_3^+$ and $(\mu\text{-H})_2(CO)_9Os_3$ Fragments[a]

MO	sym	% of Os(1)	% of Os(2) [or Os(2′)]	Os(1)–Os(2) Os(1)–Os(2′)]	Os(2)–Os(2′)
			$(\mu\text{-H})_3(CO)_9Os_3^+$		
61	a_2	21	20	ab	ab
60	e	2	32	n	ab
59	e	42	14	ab	b
58	a_1	23	23	b	b
49	a_1	29	28	b	b
			$(\mu\text{-H})_2(CO)_9Os_3$		
61	a″	21	21	ab	ab
60	a″	4	36	n	ab
59	a′	39	18	ab	b
58	a′	26	22	b	b
48	a′	39	24	b	b

[a] Key: b ≡ Os–Os bonding; ab ≡ Os–Os antibonding; n ≡ Os–Os nonbonding.

osmium triangle through Os–H–Os bonds. Orbital 57, in IV′ designated a′, has no counterpart in III′ and is derived mainly from metal orbitals.

The principal orbitals that tend to bind the capping BCO^- and CCO units are 58–60 in III′ and IV′ plus 49 for III′ and 48 for IV′. Their symmetries and contributions to metal–metal bonding are listed in Table IV. For III′ there are two orbitals of a_1 symmetry, a doubly degenerate pair of e symmetry, and one a_2 orbital. For IV′ there are three a′ orbitals and two orbitals of a″ symmetry. The HOMO of III′ is of a_1 symmetry while the HOMO of IV′ is of a′ symmetry. There is no large perturbation of the LUMO and other higher lying unoccupied MO's in going from III′ to IV′.

B. $(\mu\text{-H})_3(CO)_9Os_3BCO$ Compared to $(\mu\text{-H})_2(CO)_9Os_3CCO$. Table V presents the principal MO's involved in bonding III′ to BCO^- and IV′ to CCO. Table VI presents an analysis of the net fragment–fragment overlap populations. Correlation diagrams (Figures 8 and 9) were derived from the information given in these two tables. As expected the major interactions in the formation of IIIa involve the 4σ orbital (6) of BCO^- interacting with the a_1 orbitals (49 and 58) of III′ and the 2π orbitals (7 and 8) of BCO^- interacting with the doubly degenerate e orbital (59 and 60) of III′. The antibonding a_2 orbital (61) of III′ does not participate in bonding of the BCO^- group; it constitutes the LUMO of the molecule.

While there are some significant differences in the energy levels of IIIa and IV, the major interactions in the correlation diagrams for the formation of these clusters are analogous. Thus in the formation of IV the 4σ orbital of the CCO unit interacts with MO's 48 and 58 of IV′ and the 2π orbitals of CCO interact with MO's 59 and 60. The antibonding orbital (61) of IV′ does not correlate with CCO and therefore becomes the LUMO of the molecule.

Consider the differences between the energy levels for IIIa and IV. The HOMO of molecule IV is localized on IV′. Orbital 57 of IV′ has no counterpart in III′. The HOMO's of IIIa are doubly degenerate. In compound IIIa MO 53 involved Os_3B bonding. Its energy is between that of MO's 51, 52, and 54, which involve primarily Os–H–Os bonding. This contrasts with the energies of the analogous orbitals in IV. In this case MO 51 is the analogous orbital. It involves bonding of Os_3C, but its energy level is below that of MO's 52 and 53, which involve Os–H–Os bonding. This ordering of energy levels also occurs in the methylidyne clusters $(\mu\text{-H})_3Fe_3(CO)_9(\mu_3\text{-}CCH_3)$ and $(\mu\text{-H})_3Ru_3(CO)_9CH$. Similar differences in ordering of analogous energy levels are also observed in the butterfly tetrairon cluster systems $(\mu\text{-H})Fe_4(CO)_{12}BH_2$ and $(\mu\text{-H})Fe_4(CO)_{12}CH_2^+$, which contain a BH_2 and a CH_2^+ unit, respectively, bound to an Fe_4 unit. These differences in energy levels are probably due to the higher nuclear charge of the C atom than the B atom. This difference is reflected in

Table V. Principal Metal–Ligand Bonding MO's

$(\mu\text{-H})_3(CO)_9Os_3BCO$				$(\mu\text{-H})_2(CO)_9Os_3CCO$			
MO	E, eV	$(\mu\text{-H})_3(CO)_9Os_3^+$	BCO^-	MO	E, eV	$(\mu\text{-H})_2(CO)_9Os_3$	CCO
53	−14.6	36% 49, 11% 58	43% 6	49	−17.5	5% 40, 60% 44, 5% 48	4% 5, 21% 6
55	−12.0	45% 50	31% 7	51	−16.6	35% 44, 13% 48, 8% 58	2% 5, 32% 6
56	−12.0	45% 51	31% 8	54	−13.6	13% 50, 7% 52, 15% 59	55% 7
63	−9.4	26% 49, 23% 52, 41% 58	9% 6	55	−13.5	27% 49, 13% 60	51% 8
64	−8.8	15% 50, 16% 53, 22% 59, 9% 60	18% 7	58	−10.6	61% 49, 9% 53, 11% 55, 9% 60	9% 8
65	−8.8	15% 51, 26% 54, 9% 49, 22% 60	18% 8	63	−9.3	3% 48, 13% 50, 55% 52, 4% 47, 6% 58, 23% 59	4% 7
				64	−9.3	8% 49, 34% 53, 34% 55, 8% 56, 11% 60	4% 8

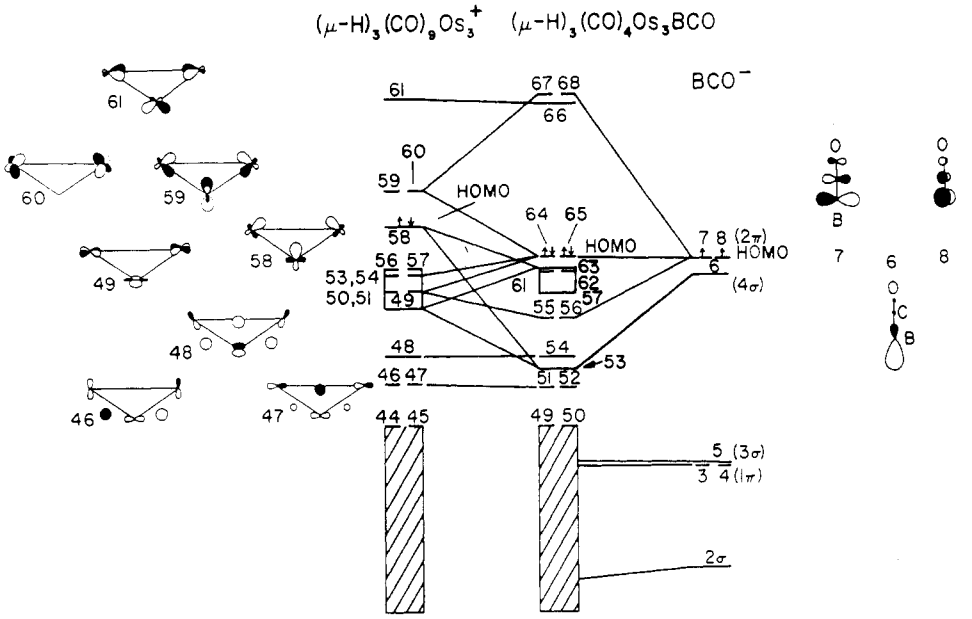

Figure 8. Fragment orbital correlation diagram for the formation of IIIa from $(\mu\text{-H})_3Os_3(CO)_9^+$ and BCO^-.

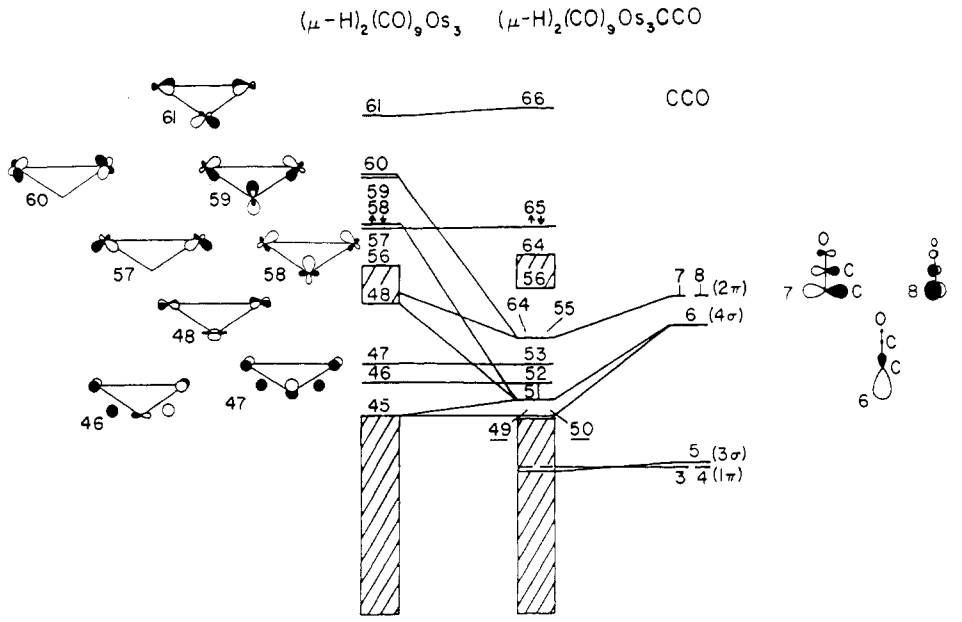

Figure 9. Fragment orbital correlation diagram for the formation of IV from $(\mu\text{-H})_2Os_3(CO)_9$ and CCO.

Table VI. Overlap Population (>0.02) between $H_3(CO)_9Os_3^+$ and BCO^- Fragments and between $H_2(CO)_9Os_3$ and CCO

$(\mu\text{-H})_3(CO)_9Os_3^+$ orbital	BCO^-		
	6	7	8
49	0.102		
52	0.022		
58	0.653		
59		0.376	0.104
60		0.104	0.376
$(\mu\text{-H})_2(CO)_9Os_3$ orbital	CCO		
	6	7	8
48	0.059		
58	0.542		
59		0.388	
60			0.378

the lower energy of the 4σ and 2π MO's of CCO compared to the 4σ and 2π MO's of BCO^- (Figures 8 and 9).

An interesting consequence of these shifts in orbital energy is that the BCO fragment orbitals are in a more favorable position to interact with the metal orbitals. The net effect is seen in Tables V and VI where the extent of mixing (from the percent orbital composition) and fragment overlap analysis clearly show that BCO fragment is interacting more strongly with the metal fragment than the CCO fragment is.

The qualitative changes that take place in the calculations on going from IIIa and IV are in excellent agreement with the experimental results discussed previously.

C. $(\mu\text{-H})_3(CO)_9Os_3BCO$ Compared to $(\mu\text{-H})_3(CO)_9Os_3BPMe_3$. In order to compare IIIa and IIIb, fragment analyses were carried out on $(\mu\text{-H})_3Os_3(CO)_9B$, CO, and PMe_3. The energy level diagram for the $(\mu\text{-H})_3(CO)_9Os_3B$ fragment is given in Figure 10. MO 61, the LUMO, is mainly derived from the p_z orbital of the capping boron atom. The capping boron atom is bound to the osmium triangle through π orbitals 59 and 60 and through σ orbital 52. MO's 50 and 51 are doubly degenerate orbitals, which are principally of p_x and p_y character.

Energy level diagrams for IIIa,b are shown in Figure 11. Contributions to the important MO's from the fragments $(\mu\text{-H})_3(CO)_9Os_3B$, CO, and PMe_3 for IIIa,b are listed in Tables VII and VIII. Overlap populations, Mulliken populations for fragment MO's and Mulliken atomic charges for these two compounds are also listed in Table VII and VIII. There are some significant

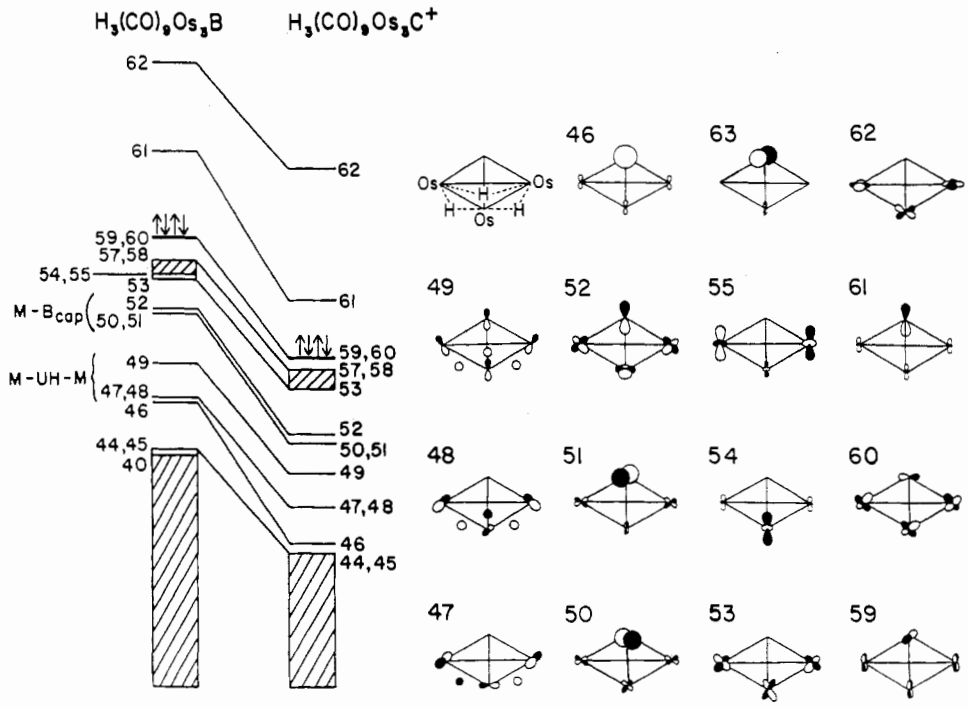

Figure 10. Orbital energy changes on going from $(\mu\text{-H})_3Os_3(CO)_9B$ to $(\mu\text{-H})_3Os_3(CO)_9C^+$ with a schematic representation of the orbitals involved.

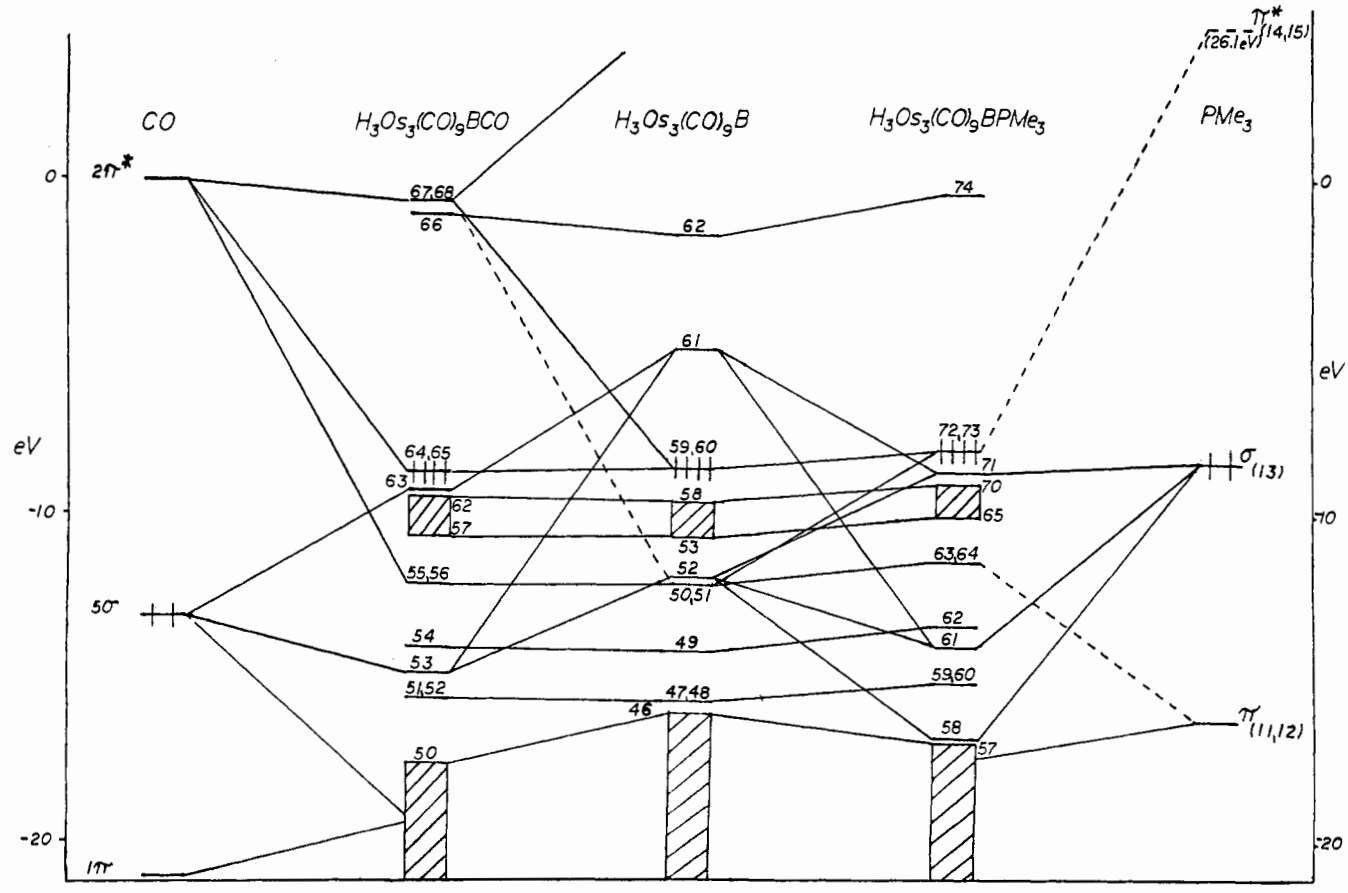

Figure 11. Fragment orbital correlation diagram for the formation of IIIa,b from $(\mu\text{-H})_3Os_3(CO)_9B$ (center) with CO (left) and PMe_3 (right).

differences between these two compounds. Generally, the MO eigenvalues of IIIb are higher than those of the corresponding MO's of IIIa. This observation is consistent with what was seen in the PES results for IIIa,b as well as the for mononuclear systems discussed. The double degenerate orbitals HOMO 64 and 65 and MO 55 and 56 of IIIa contain a significant percentage of 2π character from CO as well as contributions from the $(\mu\text{-H})_3(CO)_9Os_3B$ fragment. On the other hand, the corresponding orbitals of IIIb, MO's 72 and 73 and MO's 63 and 64, consist mainly of contributions from the $(\mu\text{-H})_3(CO)_9Os_3B$ fragment. HOMO 13 of PMe_3 contributes more to MO's 71, 61, and 58 of IIIb than the 5σ orbital of CO contributes to the analogous orbitals, MO's 63, 53, and 48 of IIIa. LUMO 61 of $(\mu\text{-H})_3(CO)_9Os_3B$ has a larger Mulliken population in IIIb (1.214) than in IIIa (1.179), while the 5σ of CO has a larger Mulliken population (1.271) in IIIa than HOMO 13 of PMe_3 (1.145) in IIIb.

Table VII. Principal Cluster–Ligand Bonding MO's as a Percentage of Fragment Character, Overlap Populations, Mulliken Fragment Orbital Populations and Mulliken Atomic Charges for IIIa as a Function of $H_3Os_3(CO)_9B$ and CO

MO	*E*, eV	$H_3Os_3(CO)_9B$	CO
11	−25.3	13% 61	45% 4σ, 18% 5σ
39 (40)	−19.5		95% $1\pi_x$ (95% $1\pi_y$)
41	−19.3	11% 37, 5% 40, 3% 46, 1% 17, 1% 61	42% 4σ, 35% 5σ
48	−17.6	4% 37, 78% 40, 8% 46, 2% 61	4% 5σ
53	−14.6	70% 46, 17% 52, 7% 61	2% 5σ
55 (56)	−12.0	80% 50 (88% 51)	7% $2\pi_x$ (7% $2\pi_y$)
63	−9.4	33% 52, 31% 53, 31% 61	1% 5σ
64 (65)	−8.8	91% 59 (91% 60)	5% $2\pi_x$ (5% $2\pi_y$)

Overlap Population (≥0.03)

	$H_3Os_3(CO)_9B$					
CO	50	51	52	59	60	61
4σ						0.048
5σ			0.102			0.539
$2\pi_x$	0.101			0.101		
$2\pi_y$		0.101			0.101	

Mulliken Population

	$H_3(CO)_9Os_3B$					
MO	50	57	52	59	60	61
	1.89	1.89	1.81	1.85	1.85	1.18

	CO			
MO	4σ	5σ	$2\pi_x$	$2\pi_y$
	1.89	1.27	0.28	0.28

Mulliken Atomic Charge

H	C	O	Os	B	C_{apical}	O_{apical}
−0.176	0.109	−0.085	0.234	−0.904	0.539	−0.246

The 2π LUMO's of CO have significant Mulliken populations in IIIa compared with the LUMO's of PMe_3 in IIIb. The Mulliken atomic charge on boron and $Os(CO)_3$ is more negative in IIIb than in IIIa. These results are consistent with each other and indicate that the PMe_3 ligand is a stronger σ donor relative to CO in complexes IIIa,b; however, CO has significantly greater π-acceptor character.

Electron density is therefore being shifted from the ligand onto the cluster fragment, causing the observed inductive shift of 0.5–0.7 eV. Also, since the boron center is the only one directly bound to the apical ligand, more negative charge is localized here, preferentially destabilizing the orbitals with boron character (71–73, 64, 63, 61) by 0.1–0.2 eV in agreement with what was predicted earlier from the mononuclear systems. The small magnitude of this preferential destabilization relative to the total inductive shift explains why it was not seen experimentally. MO's 23–32 of IIIb are derived mainly from the C–H bond of PMe_3 and have no counterparts in IIIa.

The effects of phenyl, chloro, and bromo substituents in clusters Ic–e were explored for the fragments $H_3Os_3(CO)_9C^+$ with $C_6H_5^-$, Cl^-, and Br^-. The results did not differ significantly from the PE results and so are not included in this discussion. They may be obtained as supplementary material for this work.

Conclusions

The comparison presented above points to the conclusion that, when bound to a transition-metal cluster, boron can act as a pseudo metal atom. From both PES and calculational evidence, it is apparent that orbitals of apical boron character are less stable than those of apical carbon character, owing to the smaller effective nuclear charge of boron. These orbitals are therefore in a better position to interact with the high-lying metal orbitals. Support for this point was found in the orbital character and overlap analysis where it is seen that the overlap populations and extent of orbital mixing clearly point to more interaction between the metal fragment and BCO than with CCO. The behavior of the boron center toward incoming ligands is also reminiscent of a metal cage center. The calculations indicate that a synergetic

Table VIII. Principal Cluster–Ligand Bonding MO's as a Percentage of Fragment Character, Overlap Populations, Mulliken Fragment Orbital Populations, and Mulliken Atomic Charges for IIIb from $H_3Os_3(CO)_9B$ and PMe_3

MO	*E*, eV	$H_3(CO)_9Os_3B$	PMe_3
10	−32.17		100% 1
11	−30.48		93% 2, 4% 3
12	−30.47		4% 2, 93% 3
13	−25.81	2% 46, 2% 52, 5% 61	86% 4, 2% 13
23	−22.49	22% 2	2% 4, 93% 7
24	−22.32		43% 5, 32% 6, 4% 9, 20% 10
25	−22.32		31% 5, 39% 6, 25% 9, 4% 10
26	−22.14		2% 5, 27% 6, 69% 9
27	−22.13		23% 5, 1% 6, 1% 8, 73% 10
28	−22.08	1% 27	97% 8
32	−20.73	94% 22	2% 7
37	−20.50	96% 27	1% 8
47	−19.01	28% 37, 14% 40, 12% 46, 3% 52, 3% 61	6% 4, 2% 7, 30% 13
48	−18.03	64% 37, 25% 40, 5% 46	3% 13
49	−17.94	47% 38, 46% 39	7% 12
50	−17.94	45% 38, 47% 39	7% 11
51	−17.55	2% 38, 4% 38, 5% 41, 10% 42, 1% 50	75% 11, 2% 12
52	−17.55	3% 38, 2% 39, 10% 41, 5% 42, 1% 51	2% 11, 75% 12
53	−17.20	4% 41, 75% 42, 3% 44, 3% 45	11% 11
54	−17.19	75% 41, 4% 42, 1% 43, 4% 44, 2% 45	11% 12
56	−16.99	1% 41, 3% 42, 13% 44, 81% 45	1% 11
57	−16.98	4% 41, 2% 42, 79% 44, 13% 45	1% 12
58	−16.78	6% 37, 57% 40, 22% 46, 3% 52, 2% 61	8% 13
61	−13.71	49% 46, 4% 49, 25% 52, 2% 53, 8% 61	8% 13
63	−11.24	21% 50, 76% 51	1% 11
64	−11.24	76% 50, 21% 51	1% 12
71	−8.61	31% 52, 24% 53, 38% 61	3% 13
72	−8.01 (HOMO)	97% 59, 2% 60	1% 14
73	−8.01 (HOMO)	2% 59, 97% 60	1% 15

Overlap Population (≥0.02)

	PMe_3		
$H_3Os_3(CO)_9B$	13	14	15
38	0.022		
46	0.022		
50			0.023
51		0.023	
52	0.114		
59			0.023
60		0.020	
61		0.494	

Mulliken Population

$H_3Os_3(CO)_9B$				
46	52	59	60 (HOMO)	61
1.891	1.815	1.979	1.979	1.214

PMe_3		
13 (HOMO)	14	15
1.145	0.045	0.045

Mulliken Atomic Charge

H	Os	C	O	B	P	C	H
−0.174	0.217	0.103	−0.094	−1.103	1.383	−0.468	0.090

interaction exists between the CO ligand and boron center which is analogous to that seen in metal carbonyl systems. Likewise, on going from the strongly back-bonding CO ligand to the weakly back-bonding PMe_3 ligand, PE results in conjunction with calculations show the same kind of inductive shifts observed in strictly metal systems.

Experimental Section

The compounds used in this study were prepared as previously described.[2,3,21] The He I (21.2-eV) and Ne I (16.8-eV) photoelectron spectra were recorded by using a spectrometer whose configuration has also been described previously.[1b,13] The instrument was initially calibrated by using a 50/50 mixture of Xe/Ar gas and in all cases achieved a resolution of 45 meV or better relative to Xe (fwhm). Individual band positions were determined by using Ar (15.76 and 15.93 eV) and a band resulting from a trace amount of H_2O (12.62 eV). All samples were air-stable solids at room temperature, and it was necessary to heat them in order to produce sufficient vapor pressure to obtain a spectrum. The minimal temperature necessary to achieve sublimation was used, these temperatures being 88 °C for Ic, 91 °C for Id, 94 °C for Ie, 86 °C for IIIa, 120 °C for IIIb, and 81 °C for IV. In all cases, the samples sublimed cleanly with no evidence of decomposition being seen, i.e. production of CO.

Acknowledgment. The support of the National Science Foundation (Grant CHE84-08251 to T.P.F. and Grant CHE84-11630 to S.G.S.) is gratefully acknowledged. We thank Dr. Brude E. Bursten for providing the Fenske–Hall programs.

Registry No. Ia, 69440-00-2; Ib, 63280-43-3; Ic, 90911-11-8; Id, 90911-10-7; Ie, 73746-96-0; II, 13682-04-7; IIIa, 86727-98-2; IIIb, 86728-00-9; IV, 83585-34-6.

Supplementary Material Available: Tables and figures showing the results of MO calculations on Ic–e with related discussion (7 pages). Ordering information is given on any current masthead page.

(21) Shore, S. G.; Jan, D.-Y.; Hsu, W.-L.; Hsu, L.-Y.; Kennedy, S.; Huffman, J. C.; Wang, T.-C. L.; Marshall, A. G. *J. Chem. Soc., Chem. Commun.* **1984**, 392.

Contribution from the Department of Chemistry, Florida State University, Tallahassee, Florida 32306-3006

Thermodynamics of Complexation of Lanthanides by Dicarboxylate Ligands

G. R. Choppin,* A. Dadgar,† and E. N. Rizkalla‡

Received March 3, 1986

Thermodynamic parameters of complexation of lanthanide cations by succinate, glutarate, adipate, and *trans*-1,4-cyclohexanedicarboxylate (CHDCA) ligands have been measured with potentiometric and calorimetric techniques. When analogous data for oxalate and malonate complexing are included, the complex stability decreases sharply as the ring size increases from 5 to 7; however, for 7–9-membered rings, there is little difference in stability. The negative entropy contribution associated with expansion in ring size has been attributed to an increasing loss in the configurational entropy in the alkyl chain. The more positive entropy for the Sm–CHDCA complex compared to that of Sm–adipate is attributed to the favorable boat configuration for chelation with CHDCA.

Introduction

The strongly ionic nature of the bonding of lanthanide cations in complexes leads to variable coordination numbers and geometries that reflect steric and electrostatic interactions between metal, donor atoms, and solvent. Such properties allow lanthanide cations to accomodate to a wider range of chelate rings than metals requiring orbital overlap with a fixed coordination geometry. The relation of stability and chelate ring size has been investigated for complexation of lanthanides by amino polycarboxylates. For the ligands $(^-O_2CCH_2)_2N(CH_2)_nN(CH_2CO_2^-)_2$ where n = 2 (EDTA) 3, (TMDTA) and 4 (TMEDTA), the stability as measured by the formation equilibrium (stability) constant decreased by slightly more than 2 log units for each unit increase in the N–Ln–N chelate ring size.[1] This decreased stability was associated with more positive values for both the enthalpies and entropies of formation. The data were interpreted in terms of much weaker Ln–N interaction with increasing ring size.[2]

To expand the investigation of stability and chelate ring size, we have studied the thermodynamics of complexation of lanthanides by a series of alkanedicarboxylates. The ligands investigated were succinate $(CH_2CO_2^-)_2$, glutarate $H_2C(CH_2CO_2^-)_2$, adipate $(C_2H_4CO_2^-)_2$, and *trans*-1,4-cyclohexanedicarboxylate (CHDCA).

Experimental Section

Reagents and Solutions. Stock solutions of lanthanide perchlorates were prepared and standardized as previously described.[3] The pH of the metal solutions for potentiometric measurements was adjusted to approximately 3.5 with perchloric acid. The pH for the solutions used in the calorimetric measurements was slightly higher (4.5–5.0). Stock solutions of the ligands were prepared by using analytical grade reagents, and the molarity of these solutions was determined by potentiometric titrations. The ionic strength of all solutions was adjusted to 0.10 M with sodium perchlorate as the inert electrolyte.

Potentiometric and Calorimetric Measurement. Potentiometric (pH) data were obtained by titrating the metal solutions (50.0 mL) with partially neutralized ligand solutions. The pH, after each addition of titrant, was recorded with a Radiometer assembly consisting of a digital pH meter Model PHM 84 fitted with a combined glass–calomel electrode, an ABU 80 autoburette, and a TTA-80 titration assembly. The electrode was calibrated with standard "BuffAR" solutions of pH 4.01 and 7.00. All measurements were made at 25 °C under nitrogen gas. Since concentration quotients of the stability constants are calculated, the measured hydrogen ion activity as determined from the pH was corrected to hydrogen ion concentrations in the 0.10 M ionic medium by use of 0.782 for the activity coefficient.[4]

The heats of complexation were determined by titrating the partially neutralized ligand solution into the metal solution and using an adiabatic calorimeter fitted with a Radiometer ABU 80 autoburette and interfaced to an Ohio Scientific microcomputer.[5] A thermistor detected the changes in temperature upon titrant addition. In a typical run, 50.0 mL of the metal solution was titrated with increments of the ligand solution. All the heats measured were corrected for dilution and deprotonation of the ligand. These corrections were determined in separate blank measurements.

Results

Protonation constants of CHDCA were determined by potentiometric titration with standard base (NaOH). Literature values of the acid constants were available for the other ligands.[6]

†Present address: Great Lakes Chemical Corp., West Lafayette, IN 47906.

‡On leave from the Faculty of Science, Ain Shams University, Cairo, Egypt.

(1) Choppin, G. R. *J. Less Common Met.* **1985**, *112*, 193.
(2) Choppin, G. R.; Brock, J. L. *Inorg. Chim. Acta* **1985**, *169*, 99.
(3) Choppin, G. R.; Bertrand, P. A.; Hasegawa, Y.; Rizkalla, E. N. *Inorg. Chem.* **1982**, *21*, 3722.
(4) Davies, C. W. *J. Chem. Soc.* **1938**, 2093.
(5) Caceci, M. S.; Choppin, G. R. *Comput. Chem.* **1982**, *6*, 161.

0020-1669/86/1325-3581$01.50/0